

Atomic and electronic structure of perfect dislocations in the solar absorber materials CuInSe₂ and CuGaSe₂ studied by first-principles calculations

Daniel Barragan-Yani and Karsten Albe

*Technische Universität Darmstadt, Institut für Materialwissenschaft, Fachgebiet Materialmodellierung,
Jovanka-Bontschits-Str. 2, D-64287 Darmstadt, Germany*

(Received 9 February 2016; revised manuscript received 30 December 2016; published 7 March 2017)

Structural and electronic properties of screw and 60°-mixed glide and shuffle dislocations in the solar absorber materials CuInSe₂ and CuGaSe₂ are investigated by means of electronic structure calculations within density functional theory (DFT). Screw dislocations present distorted bonds but remain fully coordinated after structural relaxation. Relaxed 60°-mixed dislocations, in contrast, exhibit dangling and “wrong,” cation-cation or anion-anion bonds, which induce deep charge transition levels and are electrically active. Analysis of Bader charges and local density of states (LDOS) reveals that acceptor and donor levels are induced by α and β cores, respectively. Moreover, there is local charge accumulation in the surrounding of those cores which contain dangling or “wrong” bonds. Thus the apparently harmless nature of dislocations is not because they are electrically inactive, but can only be a result of passivation by segregating defects.

DOI: [10.1103/PhysRevB.95.115203](https://doi.org/10.1103/PhysRevB.95.115203)

I. INTRODUCTION

The chalcopyrite Cu(In,Ga)Se₂ (CIGSe) is a widely used absorber material in thin-film solar cells [1,2]. The optical and electronic properties of this compound can be tuned by varying the Ga:In ratio, but are also strongly affected by the presence of lattice defects. Since polycrystalline CIGSe-based solar cells tend to outperform their single crystalline counterparts, some effort has been invested in understanding the physics of grain boundaries in these materials. It has been argued that atomic reconstructions and redistributions in the surrounding of grain boundaries are responsible for their apparently beneficial effect [3–7]. The influence of other extended lattice defects including twin boundaries, stacking faults and dislocations on the cell performance is, however, also not well understood. By means of transmission electron microscopy, significant dislocation densities up to 10¹⁰–10¹¹ cm⁻² were found in CIGSe based solar cells, which at the same time show power-conversion efficiencies of more than 15% [8]. This finding implies that lattice dislocations in CIGSe-based absorber materials are electrically inactive. So far, experimental studies have dealt with the properties of line defects in single crystalline CuInSe₂ and found evidence for the presence of ⟨110⟩-type superdislocations [9,10]. A recent experiment on polycrystalline samples was conducted for by Dietrich *et al.* [8]. They found full, undissociated 60°-mixed dislocations with an inserted {112} half-plane and showed that the density of dissociated dislocations and stacking faults is rather low compared to Si crystals.

In this paper, we present a theoretical study of undissociated 60°-mixed and pure screw dislocations by means of DFT calculations. After a short description of the computational method, we start by discussing the relaxed core structures and their electronic properties based on the (local) density of states (DOS). Then, we use atomic orbital theory (AOT) to reveal the origin of the observed defect states. Afterwards, we determine how charging affects the formation energy of dislocation dipoles allowing us to draw conclusions regarding the electrical activity of such extended defects. Finally, local changes in the charge density of the

neutral dipoles are studied by means of the Bader charge analysis.

II. METHODS

Calculations were performed using the VASP [11] simulation package with projector augmented-wave potentials (PAWs) for the effective potential associated to the nucleus and the core electrons. A converged plane-wave energy cutoff of 350 eV was applied. In order to satisfy periodic boundary conditions, dislocations were studied in a dipole configuration formed by two coplanar dislocations with antiparallel Burgers vector \mathbf{b} , located in the midplane of the supercell (see Fig. 1). The initial dipole structure was obtained by applying the theoretical strain distribution associated with each dislocation to an otherwise perfect structure. An elastic strain was then applied to the supercell to compensate the plastic strain produced when the dislocation dipole is introduced into the structure. The applied elastic strain used to achieve this, is given by [12,13]

$$\boldsymbol{\epsilon}^{el} = -\frac{1}{2\Omega}(\mathbf{b} \otimes \mathbf{A} + \mathbf{A} \otimes \mathbf{b}), \quad (1)$$

where Ω is the volume of the supercell, \mathbf{A} the vector associated with the area between the two dislocations and \mathbf{b} the Burgers vector, as shown in Fig. 1. Following this recipe, we created large supercells containing various dislocation types. The resulting structures have 768 atoms and a distance of ~ 28 Å between the dislocations. Relaxed dislocations structures were obtained by ionic relaxation using single k point (Γ point) and until atomic forces was below 0.05 eV/Å. The aim of studying such large structures is to minimize the interaction between dislocations, without losing the accuracy delivered by DFT.

In order to analyze the electrical activity of the relaxed dislocations, we calculated the dislocation dipole formation energy. For a dislocation dipole configuration X with total charge state q , the dipole formation energy, $E^f[X^q]$, is given by [14,15]

$$E_{\text{dip}}^f[X^q] = E_{\text{tot}}[X^q] + E_{\text{corr}}^q - E_{\text{tot}}[\text{bulk}] + q[E_F + \epsilon_{\text{VBM}} + \Delta v_{0/b}], \quad (2)$$

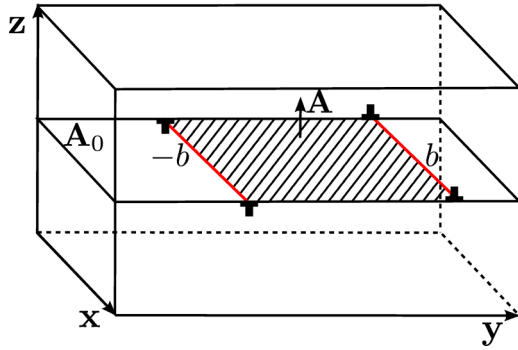


FIG. 1. Dislocation dipole configuration used to satisfy periodic boundary conditions. Red lines mark the position of the dislocations.

where $E_{\text{tot}}[X^q]$ is the total energy of the supercell containing a dislocation dipole in charge state q . E_{corr}^q accounts for the finite-size supercell correction of the interaction between localized charges in a neutralizing background. This correction refers to the image charge correction and is carried out as described by Lany *et al.* [16] using a fraction of 0.66 of the monopole correction. $E_{\text{tot}}[\text{bulk}]$ is the total energy of the nondefective and nonstrained bulk supercell, ϵ_{VBM} is the valence band maximum (VBM) energy of the perfect cell and E_F is the Fermi energy given with respect to the VBM. Finally, $\Delta v_{0/b}$ is the potential alignment correction which is obtained by a comparison between the electrostatic potential in the bulk like region far from the neutral dipole and in the bulk calculation [14]. Total energies of the relaxed structures were obtained using a converged $4 \times 1 \times 2$ Γ -centered k -point mesh and for smooth density of states we used a $4 \times 2 \times 2$ Γ -centered k -point mesh.

As implied in the definition of $E_{\text{dip}}^f[X^q]$, a given defect can exhibit different charge states depending on the value of E_F . Charge transition levels $\epsilon(q/q')$ of a given defect are defined as the Fermi energy E_F for which the formation energies of charge states q and q' are equal. They must not be confused with defect Kohn-Sham states, which are called *states* throughout this paper. Charge transition levels can be obtained as follows:

$$\epsilon(q/q') = \frac{E^f[X^q; E_F = 0] - E^f[X^{q'}; E_F = 0]}{q' - q}, \quad (3)$$

where $E^f[X^q; E_F = 0]$ is the formation energy defined in Eq. (2) when E_F is at the VBM. The transition levels are relevant because they can be directly related to experiments in which the defects are able to fully relax after the charge transition [17].

In order to obtain reliable results for $E^f[X^q]$ and $\epsilon(q/q')$, we not only have to apply finite-size corrections (E_{corr}^q) and potential alignment corrections ($\Delta v_{0/b}$), but we also have to correctly describe the band gap [16–19]. Typically, calculated band gaps obtained using computationally affordable (semi)local approximations, like LDA and GGA, are subject to severe underestimations. A correct description, like the one needed in this case, can be achieved by means of hybrid functionals or higher level theories beyond DFT [20–22]. However, these solutions are not feasible for large supercells needed to take into account the long-range strain due to the dislocation dipole. In the case of CuInSe₂ and CuGaSe₂, the

LDA calculated band gap (−0.4 eV in the case of CuInSe₂, i.e., valence and conduction bands are overlapping by 0.40 eV) is underestimated due to the incorrectly described repulsive interaction between the Cu d orbitals and Se p orbitals. This repulsion pushes the antibonding p - d valence band states to higher energies [23]. One viable way to correct this is the LDA+ U [24,25] method where an on-site Coulomb energy U localizes the Cu d orbitals. This reduces the repulsion and lowers the VBM. For the materials of interest here, a physically sensible parameter is $U_d(\text{Cu}) = 6$ eV, which correctly positions the Cu d -like valence band resonances according to photoemission experiments [26,27]. However, with this method, the band gap of CuInSe₂ is 0.12 eV and thus is still far away from its experimental value (1.04 eV).

It has been proposed in literature, to fit U parameters for different orbitals in a given compound such that the band gap is reproduced [28]. However, such solution implies forcing an unphysical localization to s and p -like orbitals, which are otherwise delocalized [17]. Although the physically driven LDA+ U method with $U_d(\text{Cu}) = 6$ eV only corrects the band gap error partially, its predicted charge transition levels can be extrapolated by a physically justified scheme proposed by Janotti *et al.* [29]. Their approach is based on the fact that defect states are a mixture of valence-band and conduction-band states. Therefore the extent to which charge transition levels change when going from LDA to LDA+ U , depends on their relative valence-band and conduction-band character. The first step for using this method is to calculate the transition level $\epsilon(q/q')$ with both LDA and LDA+ U , and then apply the following extrapolation:

$$\epsilon(q/q') = \epsilon(q/q')^{\text{LDA}+U} + \frac{\Delta\epsilon}{\Delta E_g} (E_g^{\text{expt}} - E_g^{\text{LDA}+U}) \quad (4)$$

with

$$\frac{\Delta\epsilon}{\Delta E_g} = \frac{\epsilon(q/q')^{\text{LDA}+U} - \epsilon(q/q')^{\text{LDA}}}{E_g^{\text{LDA}+U} - E_g^{\text{LDA}}}, \quad (5)$$

where E_g^{LDA} , $E_g^{\text{LDA}+U}$, and E_g^{expt} are the band gaps given by LDA, LDA+ U , and obtained by experiments, respectively. The term $\frac{\Delta\epsilon}{\Delta E_g}$ is the rate of change in the charge transition level with respect to the change in the band gap. As seen in Eq. (5), this coefficient depends on $\epsilon(q/q')^{\text{LDA}+U}$ and $\epsilon(q/q')^{\text{LDA}}$, which are the charge transition levels predicted with LDA and LDA+ U , respectively. In order to check the accuracy of this method for defects in CuInSe₂ and CuGaSe₂, we compare the charge transition levels obtained using the extrapolation method with the values obtained with a screened-exchange hybrid potential. The latter has been proven to be a reliable tool to study such systems [30]. We do so for the cation antisites, Cu_{In} and In_{Cu} in CuInSe₂, whose $\epsilon(q/q')$ are incorrectly described when using (semi)local approximations [26,31]. These calculations were performed for a supercell with 64 atoms. The calculated formation energies are shown in Fig. 2. Obviously, the positions of charge transition levels of these antisites are correctly predicted by the extrapolation method if compared to the hybrid potential calculations.

One further tool used for our study is the Bader charge analysis [32] for which we use the program of Henkelman and co-workers [33,34]. This method allows us to analyze

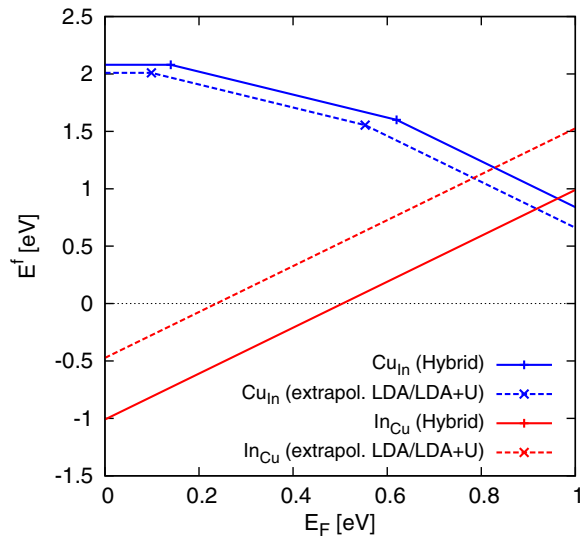


FIG. 2. Comparison between the charge transition levels of Cu_{In} and In_{Cu} antisites in CuInSe_2 obtained using an screened-exchange hybrid potential reported in Ref. [30] vs the LDA/LDA+ U extrapolation method proposed in Ref. [29].

the individual charges of the atoms in supercells containing a dislocation dipole. Visualization of the structures is done with the software tools OVITO [35] or VESTA [36]. We specify

which of the two programs was used for a specific figure in the corresponding caption.

III. RESULTS AND DISCUSSION

A. Dislocation configurations

In the chalcopyrite structure, $\{112\}$ planes have the highest packing density and therefore act as preferred slip planes for dislocations. These planes are analogues the $\{111\}$ planes in the diamond structure. In Fig. 3(a), the shaded area corresponds to a (112) plane and the minimum lattice translations are presented as red lines. From elasticity theory we know that the strain energy of a dislocation is proportional to \mathbf{b}^2 . Therefore, in this study, we are interested in the undissociated dislocations with lowest energy, i.e., dislocations with Burgers vector equal to the minimum lattice translations discussed before. Since, at least locally, the line direction \mathbf{l} is also given by lattice translations, we need to study only the screw and 60° mixed dislocation with $\mathbf{b} = \frac{1}{2}[\bar{1}10]$ and $\mathbf{b} = \frac{1}{4}[20\bar{1}]$, respectively. The line direction of both is given by $\mathbf{l} = \frac{1}{2}[\bar{1}10]$.

It is important to notice that both, screw and mixed dislocations, can either belong to glide or shuffle sets [38,39]. In Fig. 3(b), two dashed lines divide the structure and, as we will discuss, each one is associated with the glide or the shuffle set. The general structure of a screw dislocation is presented in Fig. 3(c). In there, the dislocation line is marked as a bold line

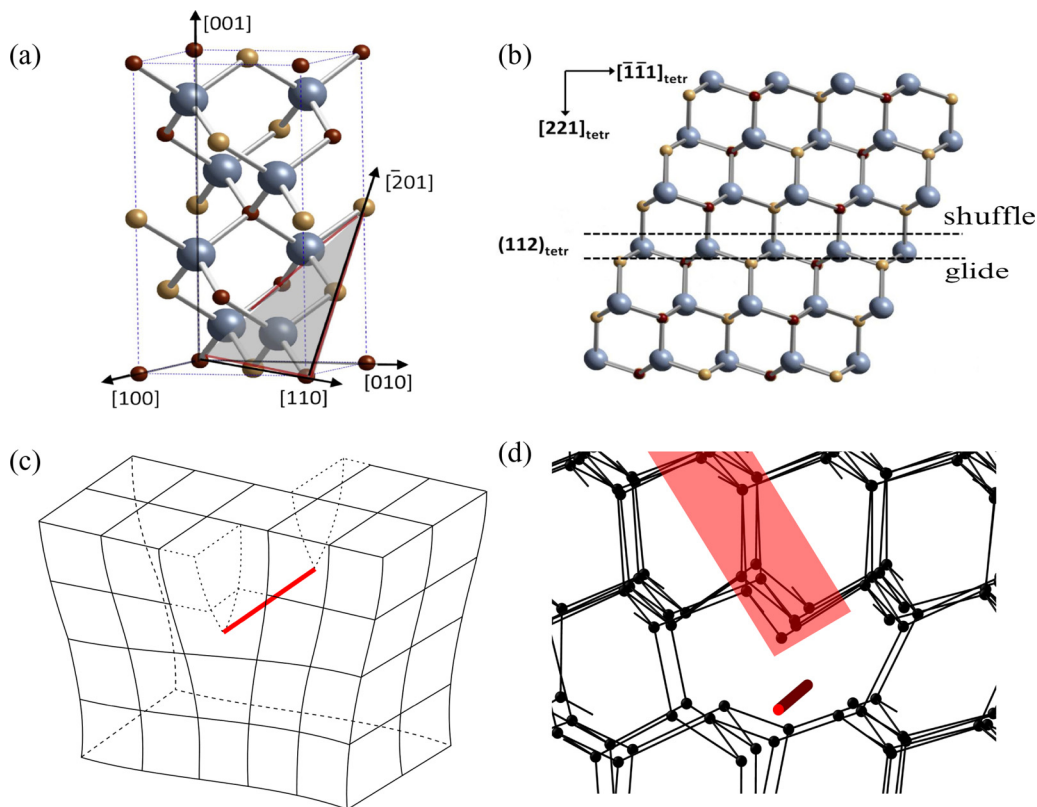


FIG. 3. (a) Ideal CuInSe_2 structure. The shaded area corresponds to a $\{112\}$ plane and the red lines show the directions associated with minimum lattice translations in the $\{112\}$ plane, from Ref. [37]. (b) Glide and shuffle $\{112\}$ planes pointed as dashed lines, from Ref. [37]. (c) General structure of a screw dislocation with line direction and Burgers vector highlighted by a red bold line. (d) General structure of a 60° mixed dislocation with highlighted inserted plane and line direction marked by a red bold line. Copper, gallium, and selenium are shown in red, blue, and yellow, respectively.

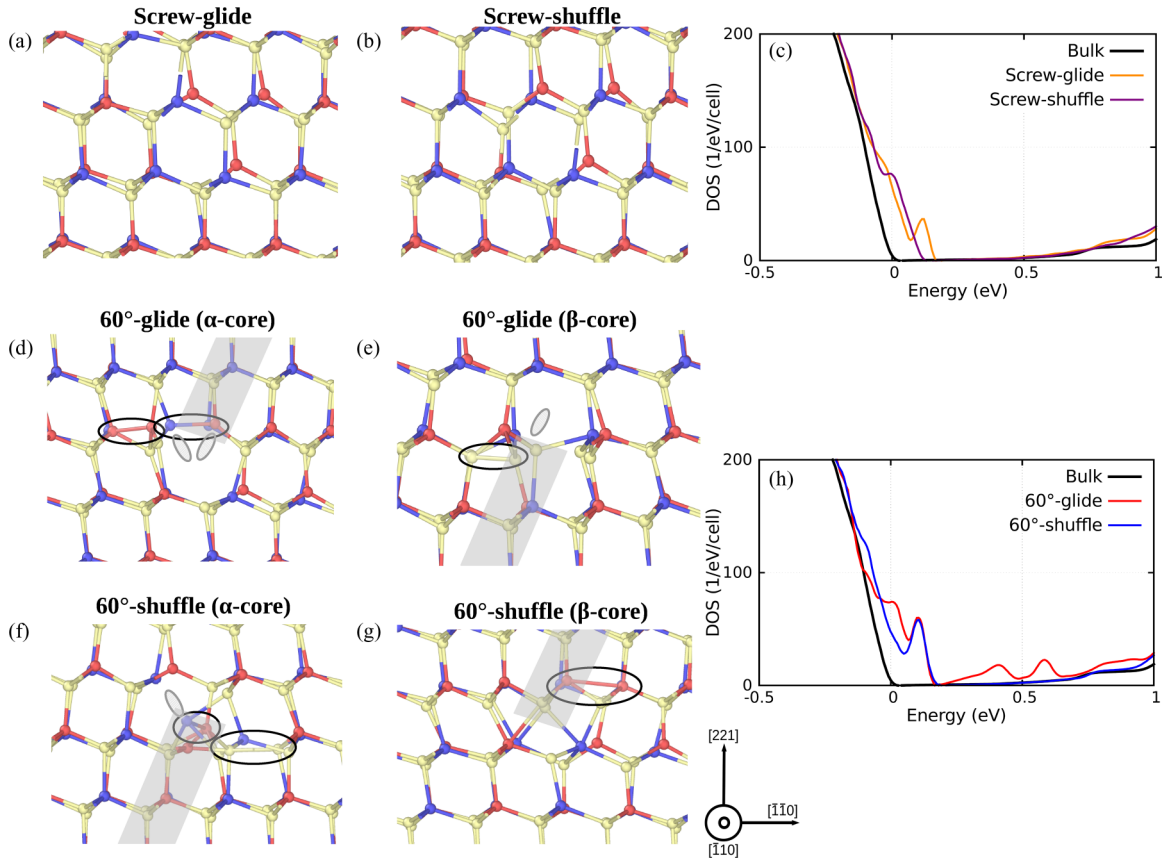


FIG. 4. Relaxed cores structures in CuInSe_2 : (a) screw glide, (b) screw shuffle, and (d) α and (e) β cores of glide 60° dislocations, and (f) α and (g) β cores of shuffle 60° dislocations. “Wrong” and dangling bonds are marked by ellipses. The ones with black boundary for the former and the ones striped for the later. Copper, indium, and selenium are shown in red, blue, and yellow, respectively. In the case of the mixed dislocations, the highlighted gray region marks the inserted half plane. Structures are visualized using OVITO. The DOS of the neutral states of these relaxed configurations are shown in (c) for the screw and (h) for the mixed dislocations. DOS are obtained from the LDA+ U calculations and are aligned with respect to core states and the VBM of the bulk structure is used as zero. The energy range is limited to the right to the experimental value of the band gap for this material (1.04 eV).

and the Burgers vector is parallel to it. Whether this dislocation type belongs to the glide or shuffle set is defined by the location of the dislocation center. It belongs to the glide set, if the center is located between two closely spaced $\{112\}$ planes and therefore is located on the lower dashed line in Fig. 3(b). On the other hand, if the center is located between two widely spaced $\{112\}$ planes, as this is the case of the upper dashed line, it belongs to the shuffle set.

In the case of 60° dislocations, we have a mixed screw and edge character. Therefore this structure exhibits an inserted plane, as it is highlighted in Fig. 3(d) by means of a shaded area. The termination of the plane inserted by the defect determines whether it is a glide or a shuffle mixed dislocation. If this inserted plane terminates on the closely spaced $\{112\}$ planes, then it belongs to the glide set. If it terminates on the widely spaced ones, then it is a shuffle. Furthermore, since the inserted plane can terminate in either a row of cations or a row of anions, we have two chemically different structures for the same dislocation set [8,40]. The cation rich structure is called α core. Analogously, the anion rich configuration is called β core. Due to the symmetry of the structure, supercells containing a dislocation dipole will thus have one α core and one β core. For CuInSe_2 (CuGaSe_2), the inserted half-plane of

an α -core 60° dislocation is terminated by copper and indium (gallium) and in the β core is terminated by selenium atoms. In the following section, the relaxed core structures of all these dislocation types and their corresponding electronic properties are discussed.

B. Atomic and electronic structures

The starting geometries, obtained from applying the displacement field of each dislocation to the supercell, are relaxed into the structures shown in Figs. 4 and 5, where only bonds shorter than 2.8 \AA are presented. The structural features observed for each relaxed core are correlated with their electronic structure. The latter is studied by means of their DOS (obtained from the LDA+ U calculations), which is presented in the same figures. As mentioned before, the LDA+ U method opens the band gap only partially. Despite this limitation, it allows us to clarify whether or not defect states are induced by the dislocations. We remark that the actual position of charge transition levels associated with the observed defect states is determined by means of the LDA/LDA+ U extrapolation method, whose results are presented in detail in the next section, Sec. III C. Whenever we refer to the conduction

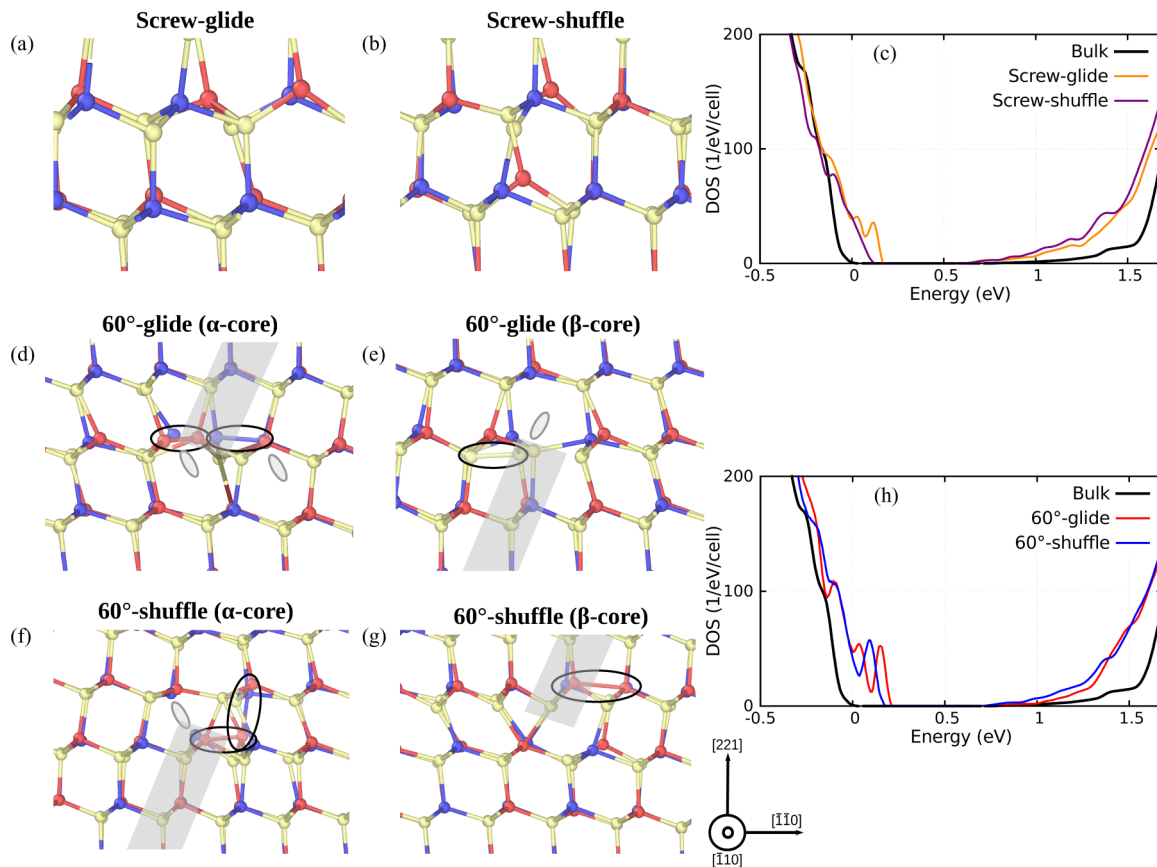


FIG. 5. Relaxed cores structures in CuGaSe_2 : (a) screw glide, (b) screw shuffle, and (d) α and (e) β cores of glide 60° dislocations, and (f) α and (g) β cores of shuffle 60° dislocations. Wrong and dangling bonds are marked by ellipses. The ones with black boundary for the former and the ones striped for the later. Copper, indium, and selenium are shown in red, blue, and yellow, respectively. In the case of the mixed dislocations, the highlighted gray region marks the inserted half plane. Structures are visualized using OVITO. The DOS of the neutral states of these relaxed configurations are shown in (c) for the screw and (h) for the mixed dislocations. DOS are obtained from the LDA+ U calculations and are aligned with respect to core states and the VBM of the bulk structure is used as zero. The energy range is limited to the right to the experimental value of the band gap for this material (1.68 eV).

band minimum (CBM) in the current subsection, we mean its experimental location, which is located at the upper limit of the energy range in all graphs showing the DOS.

We start our analysis with studying pure screw dislocations in CuInSe_2 and CuGaSe_2 , of both glide and shuffle sets. For this dislocation type, each dipole is formed by two structurally equivalent cores. Their relaxed structures can be seen in Figs. 4(a), 4(b) and 5(a), 5(b). The first point to notice is that no cation-cation or anion-anion bonds, called “wrong” bonds in the following, or dangling bonds are present in these structures. However, strain associated changes in bond lengths do exist. Using the coordination analysis tool provided by OVITO, we studied the minimum distance between atoms in the surrounding of the core compared to the bulk case. For the glide set in CuInSe_2 , this distance is 4.9% shorter compared to the bulk case, and 4.5% shorter for the shuffle dislocation. In CuGaSe_2 , the same analysis results in a 4.3% decrease in the minimum distance between atoms for the glide dislocation, and 3.2% for the shuffle dislocation. Thus, in both materials, the glide dislocation induces larger changes in the structure compared to its shuffle counterpart. The DOS of the screw dislocations in these materials, Figs. 4(c) and 5(c), present defect states close to the VBM and CBM for both the glide

and shuffle dipoles. Based on the structural analysis performed before, we conclude that these states are strain induced. A similar situation was observed for threading dislocations in GaN, where in absence of dangling bonds, a localized defect state was observed [41]. Due to the fact that compression of bonds is larger for the glide cores, defect states in this case exhibit a more pronounced detachment from the band edges. This is easy to observe for the state close to the VBM. For both, screw glide and shuffle dislocations, states close to the CBM are accompanied by a band tail caused by the strain field around the dislocation cores [42].

We continue our analysis with the 60° -mixed dislocation. In this case, there are evident differences between the glide and shuffle sets in both materials. In CuInSe_2 , the α core of the glide set, Fig. 4(d), exhibits several cations which are not fully coordinated, including the ones that terminate the inserted plane. Dangling bonds occur and there are also two “wrong” bonds (one Cu-Cu and one Cu-In) in this core. In the case of the β core, Fig. 4(e), there is one Se-Se bond and one of the Se atoms located at the termination of the inserted half plane is not fully coordinated. The latter leads to the formation of dangling bonds. The α core of the shuffle structure exhibits one dangling bond associated with the indium atom located at

the end of the inserted half-plane as well as Cu-In and Se-S bonds, Fig. 4(f).

An important point is that besides a “wrong” Cu-Cu bond, the β core of the same set, Fig. 4(g), exhibits full coordination. Performing the same analysis of the minimum distance between atoms mentioned before, we find a 5.1% and 4.5% decrease of this distance for the glide and shuffle dislocations, respectively. The DOS of these dislocation types, Fig. 4(h), shows that the shuffle structure induces defect states close to the VBM. On the other hand, for the glide set dipole we found defect states located at $\epsilon_{\text{VBM}} + 0.41\text{eV}$ and the other at $\epsilon_{\text{VBM}} + 0.58\text{ eV}$ along with a state just above the VBM and another state into the conduction band tail. In CuGaSe₂, the α core of the glide configuration contains three gallium atoms which are not fully coordinated, Fig. 5(d). Consequently, dangling bonds are formed. One of them is a gallium atom decorating the end of the inserted half plane. In addition, one Cu-Cu and one Ga-Ga bond are found. In the case of the β core, Fig. 5(e), one of the selenium atoms terminates the half-plane and is not fully coordinated, leading to a dangling bond. Furthermore, as in CuInSe₂, there is one Se-Se bond involving the very same atoms. The shuffle α core, Fig. 5(f), exhibits one dangling bond associated with the gallium atom located at the termination of the inserted half-plane as well as Cu-Cu and Cu-Ga bonds in the same structure. As it was observed for the case of CuInSe₂, besides a weak “wrong” bond (Cu-Cu), the β core of the same set, Fig. 5(g), exhibits full coordination. In this case, the minimum distance between atoms is found to decrease by 2.9% and 2.5% for the glide and shuffle set, respectively. Regarding the electronic structure, their DOS exhibits several induced defect states, Fig. 5(h). Nevertheless, in this case defect states are only found close to the VBM. Beside the induced defect states, there are other features common to both materials for this dislocation type. One feature is the existence of a large conduction band tail, which originates from the strain introduced by the dislocation. Further common features are that bond deformation is larger for the glide structures and that all defect states are localized.

C. Electrical activity and origin of defect states

In this section, we analyze the electrical activity of the various dislocations by comparing their formation energies and inspecting charge transition levels. Since every dipole of 60° dislocations consist of two different cores, one α core and one β core, their individual formation energies cannot be obtained from supercell calculations containing dipoles. Therefore formation energies considered in the following are calculated per dipole. For a particular Fermi level and dislocation type, we only display the formation energy of the charge state, per dislocation dipole, with the lowest formation energy. For clarity, we emphasize that the formation energies obtained from Eq. 2, are divided by the cell length of the relaxed structure in the direction of the dislocation line. In Fig. 6, the charge state is given by the slope of the plot and is labeled by colored numbers. We remark again that charge transition levels, $\epsilon(q/q')$, of a given defect must not be confused with the defect Kohn-Sham states. In the previous section we analyzed the defect states induced by the dislocation dipoles and their position in the DOS of the

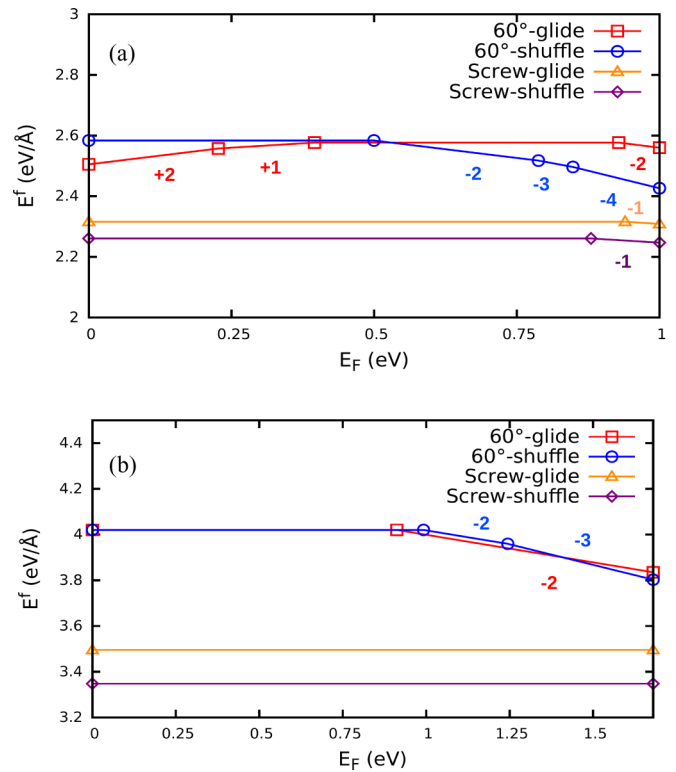


FIG. 6. Formation energies of the screw and 60° dislocation dipoles. (a) In CuInSe₂ and (b) in CuGaSe₂. Charge states are given by the slopes of the formation energy lines and for each dislocation type they are marked by numbers with corresponding color.

LDA+*U* calculation. In order to study the electrical activity of these dipoles, we use the LDA/LDA+*U* extrapolation method, which allows us to obtain accurate charge transition levels associated with the found defect states when the gap is opened up to its experimental value. For obtaining information on the origin of the transition levels, we inspect the local DOS of each core, individually.

Results for CuInSe₂ are presented in Fig. 6(a). The screw dislocations in this material have a similar behavior for both glide and shuffle sets. They are neutral when the Fermi level is below 0.93 and 0.88 eV, respectively. Above those levels, the dipoles prefer a singly negative charge state. Therefore these dislocation types introduce an extremely deep acceptor level, which is electrically harmless. One further remark is that for all charge states and both *n*-type and *p*-type conditions, the shuffle set of the screw dislocation dipole have a lower energy than its glide counterpart.

For the same material, the shuffle 60° dislocation dipole exhibits a neutral charge state until the Fermi level reaches 0.49 eV. Above that value, deep acceptor levels appear (2⁻, 3⁻ and 4⁻ charged states are stable). Therefore this dislocation pair is active for *n*-type conditions. For *p*-type conditions, this dislocation configuration prefers a neutral state. In an *n*-type sample of CuInSe₂ the shuffle configuration is always lower in energy than its glide counterpart. The case of the glide 60° dislocations is exceptional in the sense that deep donor levels are observed for Fermi energies below 0.40 eV, where 1⁺ and 2⁺ states are stable. Furthermore, a harmless extremely deep

TABLE I. Change in the Bader charge accumulated inside a cylinder around the α and β cores of the glide 60° dislocation dipole in CuInSe₂ for its possible charge states. As explained in the text, the reference used is the Bader charge accumulated inside an equivalent cylinder located in a defect free supercell.

	ΔN_e			
	+2	+1	0	-2
α core	-0.13	0.29	0.72	1.84
β core	-1.87	-1.29	-0.72	0.16

acceptor level was also found for a Fermi energy of 0.92 eV. These findings allow us to conclude that this last dislocation type is active and harmful for p -type conditions. Within the p -type regime, the glide configuration has a lower formation energy. For example, at $E_F = 0.0$ eV, the formation energy of the glide is 2.5 eV/Å, and for the shuffle, it is 2.58 eV/Å. Thus, if a 60° dislocation exists in a p -type sample of CuInSe₂, it would in principle prefer the glide configuration. However, dislocation formation is not thermally activated, but a result of the growth kinetics or strain release. Thus the formation energies only provide a measure for the excess energy needed for form one or the other.

The calculated values for CuGaSe₂ are presented in Fig. 6(b). In general, formation energies for this material do not show a strong dependence on the Fermi level, contrary to what was found for CuInSe₂. Additionally, all dislocations are predicted to be in a neutral charge state for p -type conditions. The screw dislocations, as for CuInSe₂, have a similar behavior for both glide and shuffle sets and they are neutral for all Fermi energies. Regarding the 60° dislocations in this material, contrary to what was found in CuInSe₂, both glide and shuffle sets behave in a similar way. They induce deep acceptor levels and are electrically active in the n -type regime. Furthermore, the difference in formation energies between the glide and the shuffle 60° is small for all p -type, n -type and intrinsic regimes.

These thermodynamic charge transition levels provide insights about the electrical activity of the supercells containing a dislocation dipole. However, due to the symmetry of the chalcopyrite structure, supercells containing a 60° dislocation dipole have one α core and one β core. Thus the question arises which of the two chemically different cores is associated with the acceptor levels and which with the donor ones. To answer this question, we focus on the glide 60° dislocation dipole in CuInSe₂, which exhibits both behaviors. We start by comparing the total Bader charges associated with the surrounding volumes of both cores, with respect to the Bader charge accumulated in the same volume in a defect free supercell. From this comparison, we get the change in the Bader charges ΔN_e inside the analyzed volume for different charge states. The volume assigned to a given core corresponds to the volume of a cylinder with a radius of 8 Å, whose axis corresponds to the dislocation line. This means that a volume of $\sim 30\%$ of the total volume of the supercell is assigned to each core. With that information at hand, we can establish which core receives or releases electrons while the supercell gets charged. Results of this calculation are shown in Table I. We find that around 57% of the electrons given away in the

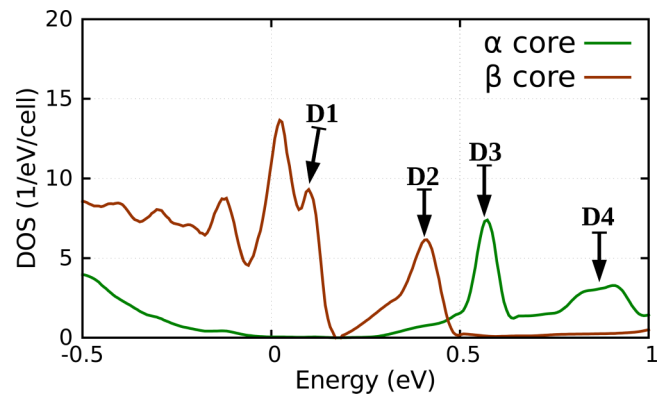


FIG. 7. LDOS of both α and β cores of the glide 60° dislocation dipole in CuInSe₂ indicating D1, D2, D3, and D4 defect states.

$2^+/1^+$ and $1^+/0$ transitions come from the β core. Regarding the acceptor level, the data suggest that around 56% of the two electrons added to the supercell in the $0/2^-$ transition are located at the α core. This gives us a first indication that acceptor states are induced by α cores and donor levels, if present, by β cores. The excess charge is not fully localized in one of the cores due to the unavoidable charge transfer between the cores in the dipole configuration we used in our study.

In the following, we used the local DOS as second and conclusive tool to clarify which of the two chemically different cores is associated with the acceptor levels and which with the donor ones. We calculated the LDOS for atoms inside a radius of 8 Å from the center of the core of α and β types of the glide 60° dislocation in CuInSe₂, Fig. 7. It is expected that $2^+/1^+$ and $1^+/0$ transitions levels are associated with the defect states close to the VBM observed for the glide 60° dislocation. By means of the LDOS, we are able to indicate which core is associated with these defect states. We find that defect states closer to the VBM, which we name D1 and D2, are induced by the β core. This provides a further proof that this core type is associated with donor levels. Analogously, it is expected that the $0/2^-$ transitions level is associated to defect states close to the CBM. From the LDOS we prove that such defect states, which we name D3 and D4, are induced by the α core confirming that this core type induces acceptor states.

Now we direct our attention to the origin of the four defect states induced by the glide 60° dislocation dipole. This analysis allows us to understand also the defect states and levels induced by the other dislocation types in these materials. In order to achieve this, we rely on the individual charge density isosurfaces of the defect states, which are shown in Figs. 8(a)–8(d). In the case of grain boundaries in CIGSe, it has been pointed out that deep defect states are induced by “wrong” bonds [43,44]. In Fig. 9, we illustrate the arguments based on atomic orbital theory (AOT) which helps us to understand the previous statement. Regarding dangling bonds, Fig. 9(a), the AOT implies that if there is a cation with a dangling bond, a donor like state will be induced and it would lie between the cation atomic s-orbital and the CBM as indicated by DBS_d (i.e., dangling bond state). In the case of an anion dangling bond, an acceptor state will be induced between the anion p -orbital and the VBM as indicated by DBS_a in the same figure. On the other hand, cation-cation or anion-anion “wrong” bonds

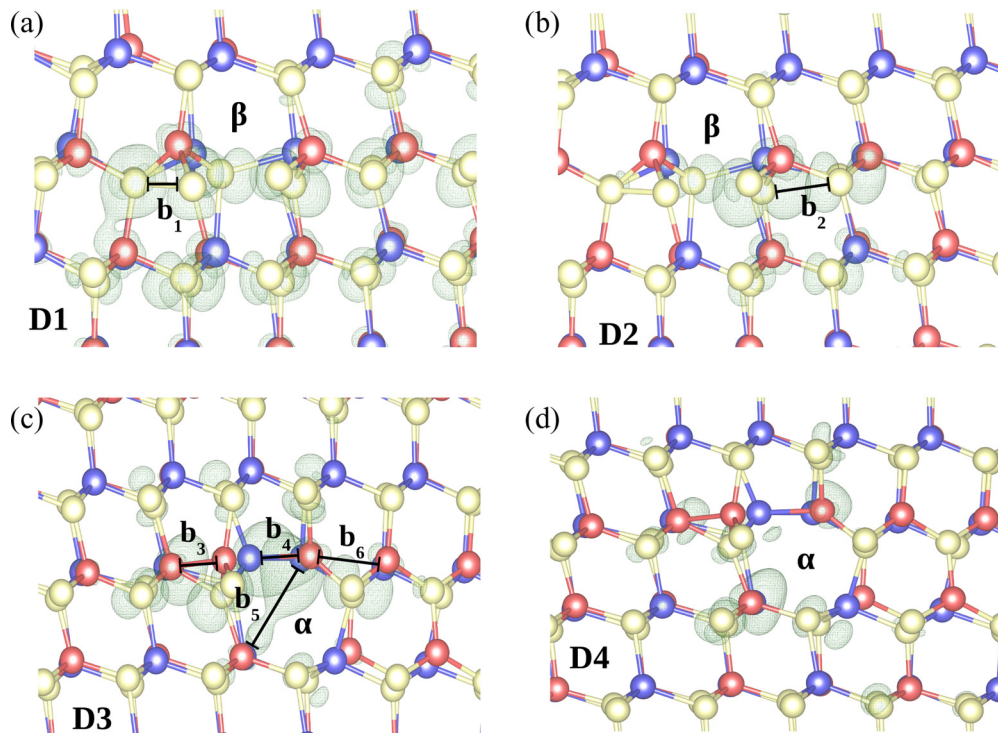


FIG. 8. Charge density isosurfaces of the defect states found for the glide 60° dislocation dipole in CuInSe_2 (a) D1, (b) D2, (c) D3, and (d) D4. The isosurfaces are visualized using VESTA and are displayed at 10% of their maximum value.

induce bonding and antibonding states which can be located deep inside the band gap, as shown in Fig. 9(b). There, bonding and antibonding defect states are indicated by WBS (i.e., wrong bond state) for the former case and WBS* for the latter. A subscript clarifies whether the WBS is induced by a cation-cation or anion-anion “wrong” bond. As stated before, the position of these defect states is driven by the lengths of the “wrong” bonds, which is directly related to the strength of the bond. We claim that dislocations induce deep defect states by means of this mechanism. As we pointed out when analyzing the structures in the previous section, several “wrong” bonds were found in the defects we are studying. In the specific case of the β core in the glide 60° dislocation dipole, there is a very noticeable Se-Se “wrong” bond highlighted in Fig. 4(e). When the isosurfaces of the defect states associated with this core are analyzed together with its structural features, we notice that defect state D1 is strongly influenced by the Se-Se bond mentioned above. In general, D1 and D2 are induced by Se orbitals. For D2, we notice that it is induced by a Se-Se bond whose existence is evident only by means of the charge density isosurfaces. On the other hand, defect states associated with the α core are caused by Cu and In orbitals. We highlight that D3 exhibits a strong influence from the Cu-Cu and Cu-In bonds mentioned before and from a bond that crosses the center of the core. This last “wrong” bond was not mentioned in the structural analysis because the simple method used then is not able to detect it. It is an In-In bond with a length of 4.35 Å, which is remarkably long compared to the In-In distance of ~ 4 Å found in the bulk. Since the distribution of “wrong” bonds is clear from the previous subsection, this analysis give also further proof that acceptor and donor levels, if present, are induced by α and β cores, respectively.

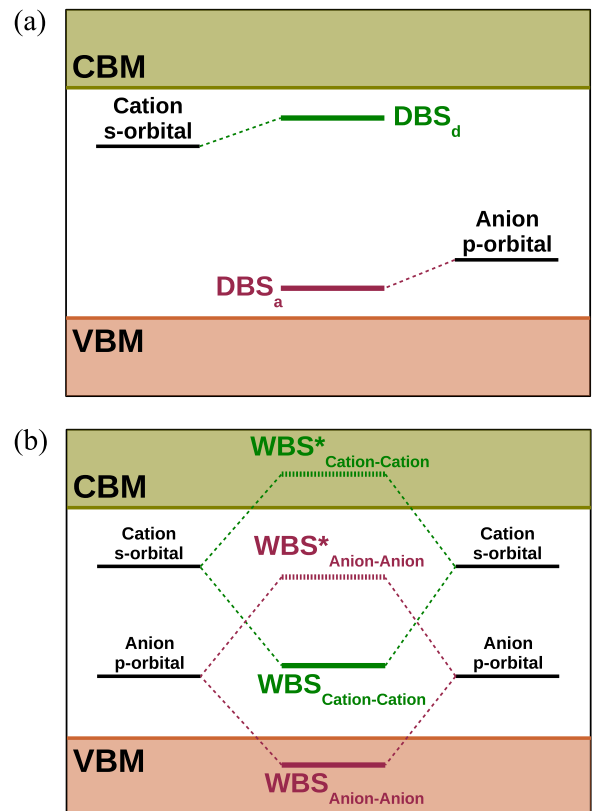


FIG. 9. Atomic orbital theory picture on the formation of defect levels in CuInSe_2 and CuGaSe_2 . (a) for dangling bond states (DBS) and (b) for “wrong” bond states (WBS). Antibonding states in the case of WBS’s are indicated by a *.

TABLE II. Comparison of relevant atomic distances within the α and β cores of the glide dislocation dipole in both CuInSe_2 and CuGaSe_2 .

	Distance (\AA)					
	b_1	b_2	b_3	b_4	b_5	b_6
CuInSe_2	2.45	3.45	2.68	2.61	4.35	3.53
CuGaSe_2	2.41	3.64	2.35	2.62	4.17	2.37

The strength of the “wrong” bonds depends on how strained they are. Therefore an analysis of their lengths provides further insights about the origin of the electronic properties found for the studied dislocations. We can now clarify why the glide 60° dislocation dipole in CuGaSe_2 does not induce defect states in the same positions as CuInSe_2 despite both relaxed cores exhibit similar features. For that matter, the length of relevant “wrong” bonds indicated in Figs. 8(a)–8(d) are reported in Table II for both materials. Each bond is designated as b_x , where the subscript x indicates a specific bond. They should not be confused with the Burgers vector of the dislocations.

We find that the Se-Se bond, b_1 , relevant for the D1 defect state and seen in both β cores is equally strong in both materials. Therefore the position of the D1 state should be the same in both materials. This is actually what is seen in the DOS of both glide dipoles, Figs. 4(h) and 5(h). However, the defect state D2 is located at different positions for each of the cores. For the CuGaSe_2 structure it is seen close to the VBM and just above the D1 state. The reason for this is that the Se-Se bond with largest contribution to that state, b_2 , is shorter in the CuInSe_2 core. Hence the WBS^* state D2 is pushed away from the VBM for that material. Electrical activity of the glide β core in CuInSe_2 is related to both D1 and D2 defect states. Since for the CuGaSe_2 core these two defect states are close to the VBM, they do not create any deep donor charge transition level for that material. Therefore it remains to answer why the position of the D3 state is also not the same for the CuGaSe_2 glide 60° dislocation dipole. As stated before, this state is associated to the α core of that dislocation type and the largest contribution to the formation of such defect state in the CuInSe_2 core comes from a Cu-Cu bond, b_3 , a Cu-In bond, b_4 , and from an In-In bond, b_5 , that crosses the center of the α core. In Table I, we report the length of these three bonds along with a cation-cation b_6 “wrong” bond which, although non existing for the CuInSe_2 structure, is important in the case of its CuGaSe_2 counterpart. Since in all cases these bonds are shorter in CuGaSe_2 , the defect state D3 (caused by bonding $\text{WBS}^*_{\text{cation-cation}}$ states) is pushed further into the band gap, close to the VBM in the LDA+ U calculation. Actually, for the glide 60° dislocation dipole in CuGaSe_2 , defects above the VBM are a mixture of D1, D2 and D3 states observed in the CuInSe_2 structure. The acceptor levels related to the D3 state are close to the CBM in CuInSe_2 . As this defect state is further apart from the CBM for CuGaSe_2 , when the band gap is opened up to its experimental value the correspondent transition levels should also get deeper into the gap compared to the CuInSe_2 case. This result is in-line with our calculated transition levels for the glide 60° dislocation dipole in CuGaSe_2 . Finally, the state D4 is induced by the same In-In bond, b_5 , that crosses the

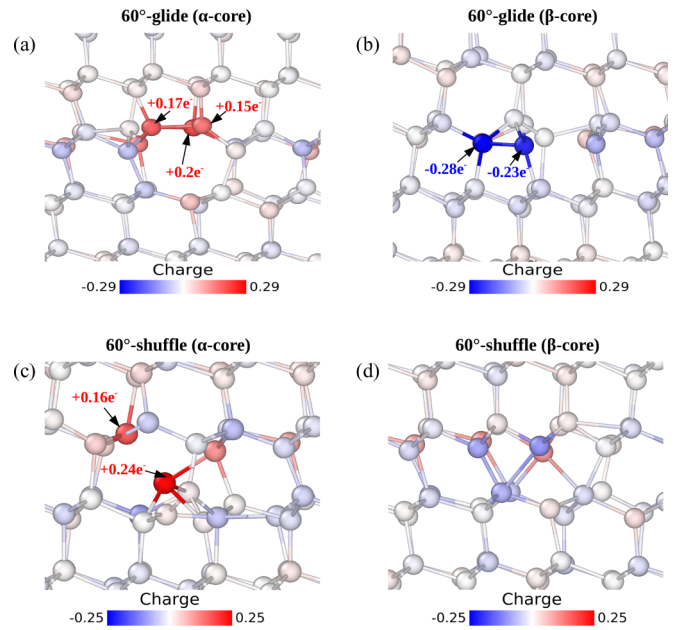


FIG. 10. Difference in Bader charges between a neutral supercell containing a 60° dislocation dipole and a defect free supercell for CuInSe_2 . (a) α core of the glide set, (b) β core of the glide set, (c) α core of the shuffle set, and (d) β core of the shuffle set. A positive or negative difference means that the atoms located at such position gained or lost, respectively, electrons in the presence of the dislocation dipole. All dipoles presented here are neutral and visualized using OVITO.

center of the core. However, it is caused by the antibonding $\text{WBS}^*_{\text{cation-cation}}$ state. Hence, due to a shorter bond length in CuGaSe_2 , this state is pushed up into the CBM and is not seen in the case of that material.

Using the AOT, we can also understand our findings for the shuffle cores. In both materials, the β cores are fully coordinated and no Se-Se bond is observed. Therefore based on the previous discussion, donor levels do not occur for these structures. Furthermore, the observed cation-cation bond in this core is a weak one and will only induce defect states close to the CBM. Structural features observed for the α cores are common in both materials. The D3-like defect state induced by that core, a strong bonding $\text{WBS}^*_{\text{cation-cation}}$ state, is pushed far apart from the CBM and is located just above the VBM in the LDA+ U calculation. Therefore the electrical activity of these cores should be like the one observed for the glide 60° dislocation dipole in CuGaSe_2 . We proved such conclusion by means of the calculated dipole formation energies, where only deep acceptor levels were found for the shuffle dipoles in both materials.

D. The meaning of the neutral state: local charge accumulation

Since we use a dipole configuration in this study, the neutral state, mentioned while analyzing the formation energy diagrams, refers to neutral supercells. However, this does not exclude the possibility of local changes in the charge density associated to charge transfer between the cores. In order to have a clear understanding of this feature, we use the Bader analysis to calculate charges associated with each atom in

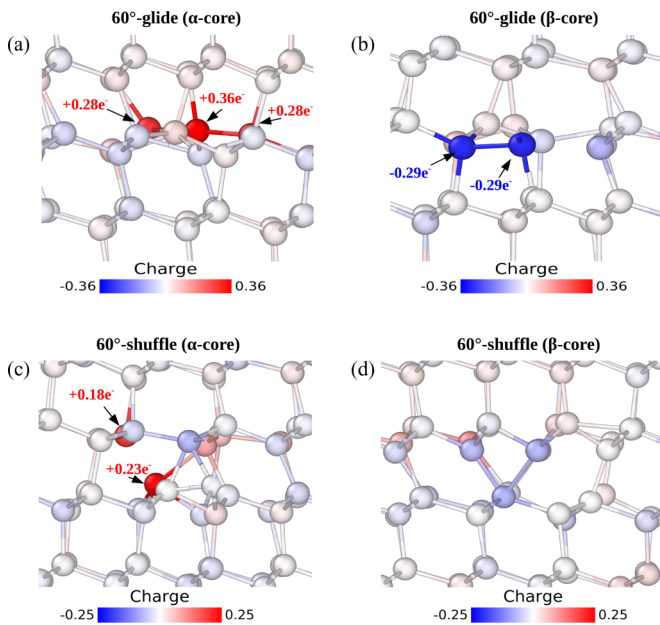


FIG. 11. Difference in Bader charges between a neutral supercell containing a 60° dislocation dipole and a defect free supercell for CuGaSe_2 . (a) α core of the glide set, (b) β core of the glide set, (c) α core of the shuffle set, and (d) β core of the shuffle set. A positive or negative difference means that the atoms located at such position gained or lost, respectively, electrons in the presence of the dislocation dipole. All dipoles presented here are neutral and visualized using OVITO.

the corresponding supercells. Differences in Bader charges between a neutral supercell containing a 60° dislocation dipole and a defect free supercell for both CuInSe_2 and CuGaSe_2 are presented in Figs. 10 and 11. Although all dipoles shown are neutral, there are indeed local changes in the charge density. In general, there is electron accumulation in α cores. The reason for this excess in “Bader charge is that for cations, each missing or wrong” bond means that less charge is given away. On the other hand, β cores of the glide set exhibit electron depletion. The reason for this is that for anions, each missing or “wrong” bond means less charge being accepted. Due to their full coordination, negligible local charge rearrangements are observed for the β cores of the shuffle set. For completeness, an analogous analysis was performed for the screw dislocations. For the neutral state, such dislocations do not show local charge accumulation or depletion in the surrounding of the cores, not even at the dislocation cores (always below ± 0.03 electrons). The relaxed structures found within this study, Figs. 4(a), 4(b) and Figs. 5(a), 5(b), explain this behavior since dangling and “wrong” bonds are not seen.

In our study, we have proven that perfect and stoichiometric dislocations in CuInSe_2 and CuGaSe_2 are electrically active. However, these defect could be passivated by point defect

segregation. Dietrich *et al.* [8] proposed Na accumulation as mechanism which explains the apparent harmless nature of dislocations in CIGSe. A key ingredient of their model is that there is accumulated charge in the cores and that segregation is driven by the electrostatic interaction between the point defects and the core. Our results support the charge accumulation premise. Consequently, we conclude that these arguments hold true for the case of 60° dislocations in CIGSe.

IV. SUMMARY AND CONCLUSIONS

We have performed first-principles calculations of relaxed dislocation cores with smallest \mathbf{b} in a chalcopyrite structure, the screw and the 60° -mixed types. In both, CuInSe_2 and CuGaSe_2 , screw dislocations present distorted bonds, but are characterized by fully coordinated cores after relaxation. On the other hand, relaxed structures of the 60° -mixed dislocations exhibit dangling and “wrong” bonds. In order to clarify whether the glide or the shuffle set is preferred, we calculated formation energies of all dipoles. Additionally, based on the position of the charge transition levels found in the dipole formation energy diagrams, we drew conclusions about the electrical activity of the dislocations under study. Our results show that in both materials, CuInSe_2 and CuGaSe_2 , screw dislocations prefer their shuffle configuration. Moreover, no deep transition level was found for this dislocation type, pointing out their harmless nature. On the other hand, deep acceptor levels were observed for most of the 60° dislocation dipoles in the n -type regime. The only exception is the glide dislocation dipole in CuInSe_2 , which exhibits two deep donor levels for the p -type regime. By means of Bader charges and LDOS we identified that acceptor and donor levels, if present, are induced by α and β cores, respectively. Furthermore, based on the AOT, we proved that deep defect states induced by the dislocation dipoles are caused by the presence of “wrong” bonds observed in the relaxed cores. Additionally, all defect states are found to be localized. In all cores exhibiting “wrong” or dangling bonds there is charge accumulation. Thus charged dislocation lines have to be passivated by segregating point defects as proposed in Ref. [8], in order to explain the apparent harmless nature of dislocations in CIGSe.

ACKNOWLEDGMENTS

The research was supported by the Helmholtz Virtual Institute VI-520 “Microstructural control of Thin-Film Solar Cells.” The authors gratefully acknowledge the computing time granted by the John von Neumann Institute for Computing (NIC) and provided on the supercomputer JUROPA at Jülich Supercomputing Center (JSC). Computational time was also made available by the HRZ (Lichtenberg-Cluster) at TU Darmstadt. The authors would like to thank J. Rohrer and A. Stukowski for fruitful scientific discussions.

[1] I. Repins, M. A. Contreras, B. Egaas, C. DeHart, J. Scharf, C. L. Perkins, B. To, and R. Noufi, *Prog. Photovolt: Res. Appl.* **16**, 235 (2008).

[2] P. Jackson, D. Hariskos, E. Lotter, S. Paetel, R. Wuerz, R. Menner, W. Wischmann, and M. Powalla, *Prog. Photovolt: Res. Appl.* **19**, 894 (2011).

- [3] C. Persson and A. Zunger, *Phys. Rev. Lett.* **91**, 266401 (2003).
- [4] Y. Yan, R. Noufi, and M. M. Al-Jassim, *Phys. Rev. Lett.* **96**, 205501 (2006).
- [5] C.-S. Jiang, M. A. Contreras, I. Repins, H. R. Moutinho, Y. Yan, M. J. Romero, L. M. Mansfield, R. Noufi, and M. M. Al-Jassim, *Appl. Phys. Lett.* **101**, 033903 (2012).
- [6] D. Abou-Ras, B. Schaffer, M. Schaffer, S. S. Schmidt, R. Caballero, and T. Unold, *Phys. Rev. Lett.* **108**, 075502 (2012).
- [7] S. S. Schmidt, D. Abou-Ras, S. Sadewasser, W. Yin, C. Feng, and Y. Yan, *Phys. Rev. Lett.* **109**, 095506 (2012).
- [8] J. Dietrich, D. Abou-Ras, S. S. Schmidt, T. Rissom, T. Unold, O. Cojocar-Mirdin, T. Niermann, M. Lehmann, C. T. Koch, and C. Boit, *J. Appl. Phys.* **115**, 103507 (2014).
- [9] C. J. Kiely, R. C. Pond, G. Kenshole, and A. Rockett, *Philos. Mag. A* **63**, 1249 (1991).
- [10] J. Hinks and S. Donnelly, *Philos. Mag.* **91**, 517 (2011).
- [11] G. Kresse and J. Furthmüller, *Phys. Rev. B* **54**, 11169 (1996).
- [12] V. Bulatov and W. Cai, *Computer Simulations of Dislocations* (Oxford University Press, Oxford, 2003).
- [13] W. Cai, V. V. Bulatov, J. Chang, J. Li, and S. Yip, *Philos. Mag.* **83**, 539 (2003).
- [14] H.-P. Komsa, T. T. Rantala, and A. Pasquarello, *Phys. Rev. B* **86**, 045112 (2012).
- [15] M. M. de Araújo, J. F. Justo, and R. W. Nunes, *Appl. Phys. Lett.* **85**, 5610 (2004).
- [16] S. Lany and A. Zunger, *Phys. Rev. B* **78**, 235104 (2008).
- [17] C. Freysoldt, B. Grabowski, T. Hickel, J. Neugebauer, G. Kresse, A. Janotti, and C. G. Van de Walle, *Rev. Mod. Phys.* **86**, 253 (2014).
- [18] A. Alkauskas and A. Pasquarello, *Phys. Rev. B* **84**, 125206 (2011).
- [19] A. Alkauskas, P. Broqvist, and A. Pasquarello, *Phys. Rev. Lett.* **101**, 046405 (2008).
- [20] W. Chen and A. Pasquarello, *J. Phys.: Condens. Matter* **27**, 133202 (2015).
- [21] H.-P. Komsa, P. Broqvist, and A. Pasquarello, *Phys. Rev. B* **81**, 205118 (2010).
- [22] W. Chen and A. Pasquarello, *Phys. Rev. B* **86**, 035134 (2012).
- [23] C. Persson, *Braz. J. Phys.* **36**, 948 (2006).
- [24] V. I. Anisimov, J. Zaanen, and O. K. Andersen, *Phys. Rev. B* **44**, 943 (1991).
- [25] S. L. Dudarev, G. A. Botton, S. Y. Savrasov, C. J. Humphreys, and A. P. Sutton, *Phys. Rev. B* **57**, 1505 (1998).
- [26] C. Persson, Y.-J. Zhao, S. Lany, and A. Zunger, *Phys. Rev. B* **72**, 035211 (2005).
- [27] S. Lany and A. Zunger, *Phys. Rev. B* **72**, 035215 (2005).
- [28] T. R. Paudel and W. R. L. Lambrecht, *Phys. Rev. B* **77**, 205202 (2008).
- [29] A. Janotti and C. G. Van de Walle, *Phys. Rev. B* **76**, 165202 (2007).
- [30] J. Pohl and K. Albe, *Phys. Rev. B* **87**, 245203 (2013).
- [31] S. B. Zhang, S.-H. Wei, A. Zunger, and H. Katayama-Yoshida, *Phys. Rev. B* **57**, 9642 (1998).
- [32] R. Bader, *Atoms in Molecules: A Quantum Theory*, International Series of Monographs on Chemistry (Clarendon, Oxford, 1990).
- [33] G. Henkelman, A. Arnaldsson, and H. Jónsson, *Comput. Mater. Sci.* **36**, 354 (2006).
- [34] E. Sanville, S. D. Kenny, R. Smith, and G. Henkelman, *J. Comput. Chem.* **28**, 899 (2007).
- [35] A. Stukowski, *Modell. Simul. Mater. Sci. Eng.* **18**, 015012 (2010).
- [36] K. Momma and F. Izumi, *J. Appl. Cryst.* **44**, 1272 (2011).
- [37] J. Dietrich, Ph.D. thesis, Technische Universität Berlin, 2013.
- [38] J. Hornstra, *J. Phys. Chem. Solids* **5**, 129 (1958).
- [39] C.-Z. Wang, J. Li, K.-M. Ho, and S. Yip, *Appl. Phys. Lett.* **89**, 051910 (2006).
- [40] X. Zhou, D. K. Ward, B. M. Wong, F. P. Doty, and J. A. Zimmerman, *J. Phys. Chem. C* **116**, 17563 (2012).
- [41] L. Lympirakis, J. Neugebauer, M. Albrecht, T. Remmele, and H. P. Strunk, *Phys. Rev. Lett.* **93**, 196401 (2004).
- [42] S. M. Lee, M. A. Belkhir, X. Y. Zhu, Y. H. Lee, Y. G. Hwang, and T. Frauenheim, *Phys. Rev. B* **61**, 16033 (2000).
- [43] Y. Yan, W.-J. Yin, Y. Wu, T. Shi, N. R. Paudel, C. Li, J. Poplawsky, Z. Wang, J. Moseley, H. Guthrey, H. Moutinho, S. J. Pennycook, and M. M. Al-Jassim, *J. Appl. Phys.* **117**, 112807 (2015).
- [44] W.-J. Yin, Y. Wu, R. Noufi, M. Al-Jassim, and Y. Yan, *Appl. Phys. Lett.* **102**, 193905 (2013).